Kuramoto synchronization of quantum tunneling polarons for describing the structure in cuprate superconductors

Kuramoto synchronization of quantum tunneling polarons for describing the dynamic structure in cuprate superconductors

Victor Velasco,[1] Marcello B. Silva Neto,[1] Andrea Perali,[2] Sandro Wimberger,[3,4] Alan R. Bishop,[5] and Steven D. Conradson[6,7]

[1]*Instituto de Fisica, Universidade Federal do Rio de Janeiro, Caixa Postal 68528, Rio de Janeiro, Brazil*
[2]*School of Pharmacy, Physics Unit, Università di Camerino, Via Madonna delle Carceri 9, 62032 Camerino, Italy*
[3]*Dipartimento di Scienze Matematiche, Fisiche e Informatiche, Università di Parma, 43124 Parma, Italy*
[4]*INFN, Sezione di Milano Bicocca, Gruppo Collegato di Parma, 43124 Parma, Italy*
[5]*Center for Nonlinear Studies, Los Alamos National Laboratory, Los Alamos, NM 87545, U.S.A.*
[6]*Department of Complex Matter, Josef Stefan Institute, 1000 Ljubljana, Slovenia*
[7]*Department of Chemistry, Washington State University, Pullman, WA 90164, U.S.A.*

(Dated: September 22, 2021)

A major open topic in cuprates is the interplay between the lattice and electronic dynamics and the importance of their coupling to the mechanism of high-temperature superconductivity (HTSC). As evidenced by Extended X-ray Absorption Fine Structure experiments (EXAFS), anharmonic structural effects are correlated with the charge dynamics and the transition to a superconducting phase in different HTSC compounds. Here we describe how structural anharmonic effects can be coupled to electronic and lattice dynamics in cuprate systems by performing the exact diagonalization of a prototype anharmonic many-body Hamiltonian on a relevant $6-$atom cluster and show that the EXAFS results can be understood as a Kuramoto synchronization between coupled internal quantum tunneling polarons associated with the two-site distribution of the copper-apical-oxygen ($\mathrm{Cu-O_{ap}}$) pair in the dynamic structure. Furthermore, we find that this first order, anti-phase synchronization transition can be fine tuned by temperature and anharmonicity of the lattice vibrations, and promotes the pumping of charge, initially stored at the apical oxygen reservoirs, into the copper-oxide planes. Simultaneously, the internal quantum tunneling polaron extends to the copper-planar-oxygen ($\mathrm{Cu-O_{pl}}$) pair. All these findings support an interpretation of the EXAFS data in terms of an effective, quantum mechanical triple-well-potential, which accurately represents the anti-phase synchronization of apical oxygens displacements and lattice-assisted charge transfer to the $\mathrm{CuO_2}$ plane.

I. INTRODUCTION

A series of recent reports on highly overdoped superconducting cuprates prepared by high pressure oxygen (HPO) methods have described exceptions to the structural characteristics common to O_2-oxidized materials, namely: oblate Cu geometry and inversion of the Cu $3d_{z^2-r^2}$ and $3d_{x^2-y^2}$ energies in $\mathrm{Ba_2CuO_{3.2}}$ [1]; extension of the superconductivity without a decrease in their $50-115\ K$ transition temperatures through excess Cu charge values even beyond 0.6 which far exceed the 0.27 limit of the "dome" in the conventional phase diagram [2]; in $\mathrm{Sr_2CuO_{3.3}}$, copper oxide planes as $\mathrm{CuO_{1.5}}$ instead of $\mathrm{CuO_2}$ [3] and a structural transformation concomitant with the superconducting transition[4]. This unique superconducting behavior represents an important deviation from standard BCS theory in which the mediation of Cooper pair formation by a soft vibrational mode precludes changes in the global structure in the superconducting state.

These same experiments, however, identify a remaining factor universal to high temperature superconductivity (HTSC), namely, the Internal Quantum Tunneling of (small) Polarons (IQTPs). IQTPs are a contributor to the dynamic structure, $S(Q,E)$. This quantity is easily intuited in liquids, where the positions of atoms in rapid transit between quasi-stable relative locations are identified in the van Hove function derived from inelastic scattering data [5]. X-ray Absorption Fine Structure (XAFS) spectroscopy obtains this dynamic structure via its sensitivity to the instantaneous structure factor, $S(k,t=0)$ [6, 7]. In the cuprates that are crystalline solids certain $\mathrm{Cu-O}$ pairs will exhibit a longer distance when one of the excess holes resides on the O (a lattice-assisted charge transfer within a polaron) and a shorter one when it does not, resulting in a two site distribution that does not perturb the average crystal structure. Sets of these $\mathrm{Cu-O}$ pairs, which could be two oxygen atoms bonded to the same copper, exchange these positions and charges by quantum tunneling, providing the dynamic component of the IQTP. Since the tunneling is a quantum process, the characteristic tunneling frequency is nominally temperature independent, in contrast to better known polaron transport dynamics such as thermally activated hopping. For small polarons this is much slower and therefore associated with the static structure of the material.

The initial observations of IQTPs found their signature two-site distributions in the apical $\mathrm{Cu-O}$ ($\mathrm{O_{ap}}$) (Fig. 1a) [8–14], subsequently in the planar oxygen ($\mathrm{O_{pl}}$) of the $\mathrm{CuO_2}$ planes in some compounds [15–22], and even in other HTSC materials [23–25]. Although their presence was corroborated by inelastic neutron scattering measurements [26, 27], the relative ease of XAFS measurements has caused almost all reports to utilize that method. XAFS at multiple temperatures has therefore shown the partial collapse of the associated double well in the pertinent $\mathrm{Cu-O}$ distributions across the superconducting transition, demonstrating their coupling to HTSC. Extending these experiments to compounds in which Co, Mn, and Ni are substituted for a fraction of the Cu went further, demonstrating that the IQTPs contribute to HTSC [28]. In addition to XAFS, there are numerous observations of anomalous phonons, some with distinct O-isotope dependence, in the $E < 100\ meV$ range in infrared(IR) [29–31], Raman

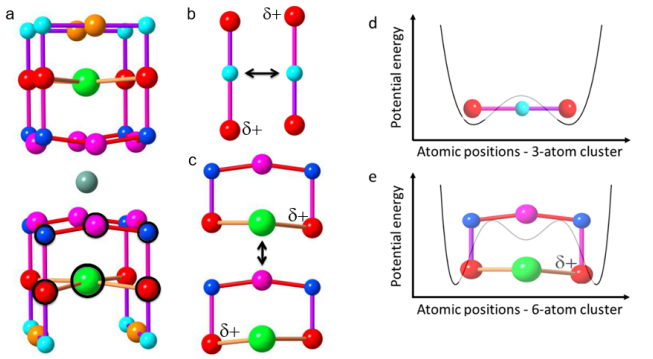

Figure 1. Relevant structures. a) The $YBa_2Cu_3O_7/YSr_2Cu_3O_7$ crystal structure shows the generic features of multilayered cuprates with higher T_c's: two, conducting CuO_2 planes (blue Cu2 and magenta Opl atoms) bridged by the intervening Y (grey), the charge reservoir consisting in this class of materials of $Cu-O$ chains (turqoise Cu1 and orange O), and the "inert" dielectric layer composed of the O_{ap} (red) and Sr (green). b) The original three atom IQTP derived from the two-site $Cu1-O_{ap}$ distribution found in $YBa_2Cu_3O_7$ showing its oscillations between its two configurations denoted by the location of the extra hole and associated longer $Cu-O$ distance($+\delta$) [7]. c) The atoms circled in black in (a) form the six atom cluster used here. Its excess charge and displacement tunnel between the two $Cu2-O_{ap}$ pairs through the O_{pl} charge-transfer-bridge. d) While for the 3-atom cluster the potential energy corresponds to a double-well dynamical, tunneling structure [11], we have found that, e) for the 6-atom cluster, the potential energy actually corresponds to a triple-well structure where the depth of the middle well is controlled by the Sr-related anharmonicity.

[32], neutron scattering [33], photoemission [34–37], and resonant inelastic x-ray spectroscopies [38–40]. The important aspect of IQTPs as a unifying element is the indication of strong, non-adiabatic, complex electron-phonon/lattice coupling.

Exact diagonalization calculations of the minimal, three-atom, O-Cu-O IQTP (Fig. 1b) [6, 11–13, 41] corroborated the experimental results and validated this approach for incorporating local quantum tunneling dynamics. More recent calculations examining fluctuating stripes within the CuO_2 planes [42] and the role of the cation on the opposite side of the O_{ap} from the Cu [43] also included dynamical contributions. Although these reports represent a substantial advance in the treatment of the lattice, they do not address the anharmonicity and its manifestation in the double well potential and its IQTPs. We do so here via two expansions of the original three-atom calculations, in a way suggested by recent data. The first is to double the number of atoms in the cluster by connecting a second Cu-O pair to the first with a planar oxygen and adding the Sr (Ba) ion that links the apical oxygen sites in the dielectric layer (Fig. 1c). We show that, under certain conditions, the addition of the planar site, O_{pl}, causes the double well potential of the three-atom cluster (Fig. 1d) to enlarge to a triple well (Fig. 1e). This occurs through the presence of the Sr atom, and specifically through a soft, molecular mode of the $O-Sr-O$ atoms. Experimental evidence for the requisite of Sr anharmonicity [44] and its coupling to the O_{ap} atoms begins with the $Cu-O_{ap}$ two-site distribution and the renormalization of the underlying double-well potential of the IQTP with temperature in, e.g., $YSr_2Cu_{2.76}Mo_{0.25}O_{7.54}$ [4] (Fig. 2a). The anomalous softening with decreasing temperature of the $Cu2-Sr$ pair beginning at T_c is apparent in the Fourier transform modulus of its EXAFS (Fig. 2b). The metrical results determined from Fig. 2a, the two $Cu-O_{ap}$ distances and the difference in the numbers of O_{ap} atoms at the shorter and longer $Cu-O_{ap}$ distances, divide into the normal state region, a fluctuation region beginning at or slightly above T_c and extending a few Kelvin below, and, as the temperature is further lowered, two more regions in the superconducting state (Fig. 2c). The $Cu-Sr$ EXAFS modulus amplitude, including its abrupt features, breaks identically, displaying a remarkably close correspondence to the numbers-of-atoms-difference curve.

Our six-atom cluster has been evaluated from four different perspectives. First, we exactly diagonalized the associated quantum many-body Hamiltonian incorporating these additional structural ingredients. We find that the anharmonicity related to the unusual dynamical structure observed in the EXAFS spectrum of Sr/Ba based cuprates is due to its vicinity to a first order synchronization transition of the IQTPs correlated with the two-site $Cu(2)-O$ pair distribution. Second is the realization that an advantageous approach to what is now effectively a system of oscillators could be adapting the Kuramoto treatment of networks [45]. This has not previously been attempted in a crystal because of the complex network of couplings through the multiplicity of phonons and because it is an application to a quantum system. In order to provide physical meaning to such a first order transition, we mapped the combined, linearised Heisenberg's equations of motion for the anharmonically coupled phonons to a mean field Kuramoto equation describing the synchronization of IQTPs within the cluster. The mapping includes both the IQTP anharmonic coupling as well as temperature/dissipation (through thermal disorder) and yields a first order syncrhonization transition to the anti-phase motions of the two IQTPs. Surprisingly, we find that in the synchronized phase charge is pumped from the apical positions into the conducting CuO_2 plane while, simultaneously, a Sr-related, triatomic molecule vibration develops a finite projection also in the copper oxide plane. This is a novel planar IQTP, associated with $Cu-O_{pl}$ deformations. Third, we have confirmed the numerical results by performing a multimodal, nonlinear Bogoliubov transformation and indeed demonstrated a polaronic degree of freedom associated with the coupling between excess charge in the plane and a new, anharmonicity-related, lattice vibration. Finally, we have observed that all of our theoretical and numerical results can be elegantly summarized as supporting a description of the EXAFS data in terms of an effective quantum mechanical triple-potential-well model (Fig. 1e). This represents an anharmonic structural adiabatic passage (ASAP) promoting anti-phase IQTP synchronization and internal charge transfer.

The paper is organized as follows: In Sec. II we describe the here proposed extension of the three-atom, $O-Cu-O$ IQTP chain into the 6-atom cluster and the numerical method-

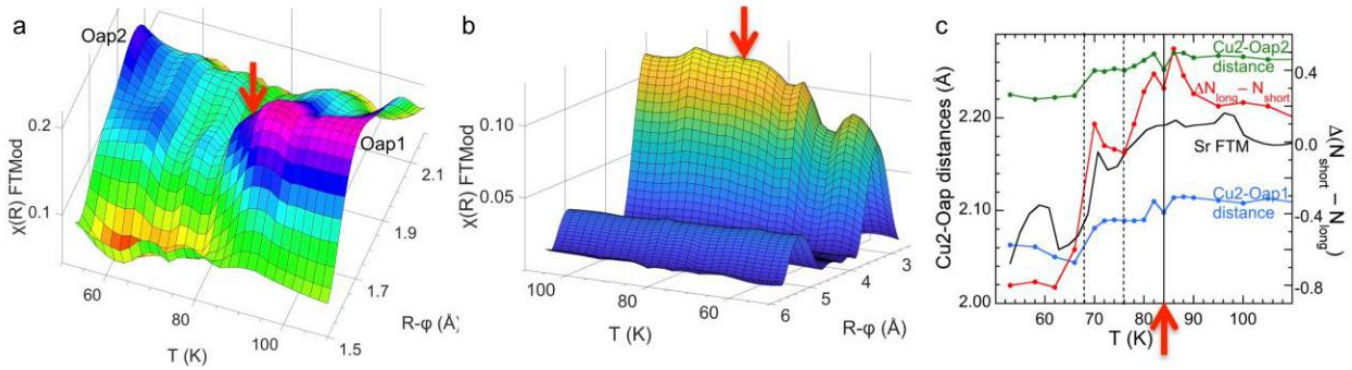

Figure 2. $E||c$ EXAFS $\chi(R)$ Fourier transform moduli of the IQTP constituents from $YSr_2Cu_{2.76}Mo_{0.25}O_{7.54}$ [2]. a) After subtraction of the principal $Cu1-O_{ap}$ contribution, the broad modulus feature that is the contribution of the two-site $Cu2-O_{ap}$ pair is apparent at $R = 1.8 - 2.2\mathring{A}$. The abrupt shift at the superconducting transition at $84\ K$ (red arrow) caused by a change in the relative numbers of apical oxygen atoms in the two sites is evident. b) The same procedure gives the $Cu2-Sr$ EXAFS contribution. Its substantial reduction in amplitude beginning at T_c contrasts with the conventional slight reduction of the Debye-Waller factor and resulting increase in amplitude displayed by the feature at $R = 5\mathring{A}$ and demonstrates the superconductivity-coupled anharmonicity of this atom pair. c) Renormalization of the $Cu2-O_{ap}$ double well potential at and below the superconducting transition causes shifts in the two $Cu2-O_{ap}$ distances (green and blue) and in the numbers of O atoms populating the two sites (red). Following the relatively constant values in the normal state, the fluctuation region between T_c and $76\ K$ displays a more continuous change in distances and numbers of atoms followed by another plateau and abrupt change at $68\ K$ prior to another flat region. Superimposing the $Cu-Sr$ Fourier transform peak amplitude from (b) (black line) shows that it tracks the same variations, demonstrating that the Sr anharmonicity is strongly coupled to the $Cu2-O_{ap}$ potential.

ology used to diagonalize its Hamiltonian. In Sec. III the numerical results are presented and discussed within the approach of the Kuramoto model for synchronization of the IQTP's, in terms of the anharmonicity, and present the nonlinear multimodal Bogoliubov transformation and the triple-well interpretation. Finally, Sec. IV is devoted to the conclusions.

II. EXACT DIAGONALIZATION

We started by performing the exact diagonalization for the extended 6-atom cluster shown in Fig. 1c). As discussed previously, the cluster was carefuly chosen to include two important structural ingredients: (i) a $Cu-O_{pl}-Cu$ charge transfer bridge, associated with a nearby, planar oxygen(O_{pl}) atom, promoting the transfer of the extra hole and longer $Cu-O_{ap}$ distance between the two lateral $Cu-O_{ap}$ IQTPs through the CuO_2 plane; and (ii) a $O_{ap}-Sr-O_{ap}$ triatomic molecule, associated with a nearby Sr atom, promoting the anharmonic coupling, referred to as K, between the apical oxygens locations of the two lateral $Cu-O_{ap}$ IQTPs through the non-charge transfer Sr atom. Notice that while the transfer included in (i) favours charge delocalization, the formation of a tri-atomic molecule, included in (ii), favours the locking of the phases of vibration above a critical anharmonicity K_c. As a result of the above rich structure, it is natural to expect that, as anharmonicity is fine tuned accross the cluster, regimes where the excess charge becomes delocalized and vibrations become synchronized are not only to be expected, but, as we are about to show, remarkably interconnected. This process ultimately provides meaning to the anharmonicity-related data observed in EXAFS as discussed previously.

The intricate interplay between lattice and charge degrees of freedom described above can be captured by the following Hamiltonian $H = H_{el} + H_{ph} + H_{el-ph} + H_{Sr}$ composed of four terms

$$H_{el} = \sum_i \varepsilon_i n_i + t \sum_{\langle ij\rangle\sigma} c^\dagger_{i\sigma} c_{j\sigma} + h.c. + U \sum_i n_{i\uparrow} n_{i\downarrow} \quad (1)$$

$$H_{ph} = \hbar\omega b^\dagger_L b_L + \hbar\omega b^\dagger_R b_R, \quad (2)$$

$$H_{el-ph} = \lambda n_L \left(b^\dagger_L + b_L\right) + \lambda n_R \left(b^\dagger_R + b_R\right), \quad (3)$$

$$H_{Sr} = \hbar\Omega_{Sr}\beta^\dagger\beta + K\left(\beta^\dagger b_L b_R + \beta b^\dagger_L b^\dagger_R\right). \quad (4)$$

In the electronic part Eq. (1), $c^\dagger_{i,\sigma}$, $c_{i,\sigma}$ are the usual creation and annihilation operators for holes with spin projection σ, with $i = 1,\ldots,5$ representing the $O_{ap}-Cu-O_{pl}-Cu-O_{ap}$ charger transfer sites, respectively, $n_i = \sum_\sigma c^\dagger_{i,\sigma} c_{i,\sigma}$ is the number occupation operator for holes at sites i, with site energies $\varepsilon_1 = \varepsilon_3 = \varepsilon_5 = -\varepsilon_2 = -\varepsilon_4$, t is the spin-preserving, nearest-neighbour hopping amplitude, and U the on-site Coulomb repulsion to prevent double occupancy. The site energies were chosen so that out of a total of three holes, as considered in this work, two of them will always be favoured at the two Cu atomic positions, while only a single, remaining excess hole minimizes the total energy by moving among the oxygen atoms while avoiding the two copper atomic positions. The phonon part Eq. (2) consists of the two harmonic infrared oscillators, of identical normal frequencies ω whose creation and annihilation operators $b^\dagger_L$, b_L, and $b^\dagger_R$, b_R represent the two possible lateral $Cu-O_{ap}$ positions, to the left (L) and to the right (R), in the cluster. The electron-phonon interaction term Eq. (3) describes the cou-

pling between the hole degrees of freedom to the lattice displacements, and the coupling constant λ (the same for either left and right) has been chosen to be large enough to ensure that polarons are formed. This is the non-adiabatic regime for polaronic formation and it was inspired by previous analogous works [13] that considered a 3-atom cluster. The novelty here is Eq. (4), which was designed to provide the cluster with a nontrivial, $\mathrm{O_{ap}} - \mathrm{Sr} - \mathrm{O_{ap}}$ triatomic molecule structure, motivated by the coupling of the anharmonicity of the neighboring Sr to the behavior of Oap atoms and the superconductivity. To describe the normal modes of vibration of the triatomic molecule we have introduced creation(annihilation) operators $\beta^\dagger$ (β) for a moderately stiff harmonic molecular phonon of normal frequency, $\Omega_{Sr} \gg \omega$. As we can see from Eq. (4) the new interaction term between the molecular phonons and the rest of the cluster is indeed anharmonic, in the form of a three-phonon coupling, and controlled by an anharmonic coupling, K. This interaction term can be interpreted as a molecule formation term, and K as a chemical potential that controls processes in which left and right phonons are destroyed to form a molecular mode, $\beta^\dagger b_L b_R$, as well as a destruction of a molecular vibration to produce left and right independent oscillations, $\beta b_L^\dagger b_R^\dagger$. As such, one would naturally expect that such a molecule formation interaction would work towards promoting the locking of phases for the apical oxygen vibrations, or equivalently, as we shall demonstrate, the synchronization of Kuramoto oscillators. For this reason the anharmonicity coupling, K, will be referred to as the Kuramoto coupling.

The exact diagonalization of the full Hamiltonian, for the ground and excited states, was perfomed using a basis of wavefunctions given by

$$|\Psi\rangle = \sum_{i,\gamma,\beta,\delta} \alpha_{i\gamma\beta\delta} \, |n_i\rangle \, |n_\gamma\rangle \, |n_\beta\rangle \, |n_\delta\rangle \, , \tag{5}$$

corresponding to a $n_{el} \times n_L \times n_R \times n_{Sr}$ dimensional Hilbert space. For the electronic states $|n_i\rangle$ we wrote down the associated Lin's table for all possible spin-up and spin-down configurations at the five charge transfer sites and a total of three holes added to the cluster. However, as discussed above, since only a single (excess) hole is found to transfer over the five charge transfer sites while the other two are favoured at the copper sites, our table was limited to a total of $n_{el} = 28$ electronic states in the occupation representation, divided into spin sectors $|n_1, n_2, n_3, n_4, n_5\rangle_\uparrow |n_1, n_2, n_3, n_4, n_5\rangle_\downarrow$ (for short, we also use $|n_1, n_2, n_3, n_4, n_5\rangle$ across the text). The $|n_\gamma\rangle|n_\beta\rangle|n_\delta\rangle$ states were written in a bosonic occupation number representation for a total of $n_L = n_R = n_{Sr} = 5$ left, right and Sr molecular phonons, respectively, justified by continuosly enlarging the phonon Hilbert subspace, through a systematic increase of the number of phonon modes until convergence.

For the numerical parameters in the Hamiltonian (1)-(4) we used [13] $\varepsilon_{1,3,5} = -\varepsilon_{2,4} = 0.5 \; eV$, favouring holes at the Cu atoms, $t = 0.5 \; eV$, and $U = 7.0 \; eV$. Furthermore, in order to fix the value of the infrared electron-phonon coupling, λ, we first exactly diagonalized a simplified version of the Hamiltonian, without the anharmonic term, $K = 0$, and searched for the crossover from adiabatic to non-adiabatic regimes, as a function of λ, to make sure the lateral polarons were formed. We have then set the value $\lambda = 0.03 \; eV$ deep inside the non-adibatic regime and we have chosen the stiff, triatomic molecule frequency, $\Omega_{Sr} = 0.14 \; eV$, to be at least twice the value of $\omega = 0.06 \; eV$.

III. NUMERICAL RESULTS AND DISCUSSION

In Fig. 3 we summarize the results obtained from our numerical, exact diagonalization studies. Figure 3a) shows the ground and two representative excited states energies as a function of the reduced coupling, K/K_c. For the ground state (black squares) one observes a clear kink at $K/K_c = 1$ while for all higher excited states (blue crosses and red circles) the kinks occur at $K/K_c < 1$. We interpret this indicating that phase locking and synchronization occur more easily for higher excited states than for the ground state. Figure 3b) shows the electronic occupations at the left (black squares), central (red circles), and right (blue crosses) sites, also as a function of the reduced coupling, K/K_c, for the ground state, which, within the Lin's table representation, can be labeled as $|11010\rangle$, $|01110\rangle$ and $|01011\rangle$, respectively. At the critical coupling, K_c, we have found a delocalization transition of the excess hole, as anticipated. In fact, while prior to the transition the hole wave function had weight only at either the left or right apical oxygen atoms, indicating formation of localized polarons, above K_c the electronic occupation for the central (planar) oxygen atom begins to increase monotonically while both the left and right occupations decrease. The abrupt discontinuity demonstrates that the phase transition is first order and this behaviour indicates the formation of what we call a *split-polaron.* Finally, Fig. 3c) shows the occupations of Sr-related, molecular phonons at the left (black squares), right (blue crosses), and central (red circles) positions within the cluster. As is evident, when K crosses K_c a novel planar lattice mode develops in the form of a sudden jump of the central Sr-related molecular phonon occupation, while the occupations of the other Sr-related phonons at the lateral positions decrease. The number of central Sr-phonons shows an abrupt jump at the critical coupling, which is again the signature of a first order phase transition.

The numerical results reveal three important features associated with the Hamiltonian (1)-(4) as anharmonicity, encoded in the Kuramoto parameter K, is varied, as shown in Fig. 4: (i) it produces a first order synchronization phase transition associated with the anharmonicity-related, triatomic molecular locking or synchronization of the phases of vibration corresponding to the two $\mathrm{O_{ap}}$ locations or $\mathrm{Cu} - \mathrm{O_{ap}}$ distances when the Kuramoto parameter K is increased (Fig. 4a); (ii) a novel extension of the IQTP into the $\mathrm{CuO_2}$ plane that results from the pumping of charge initially restricted to the Oap atoms into the copper oxide planes and delocalized througout the 6-atom cluster, while simultaneously producing a Sr-related planar oxygen displacement (Fig. 4b); and (iii) it generates a polaronic tunneling frequency that also evolves with K (Fig. 4c). In order to address each one of these issues

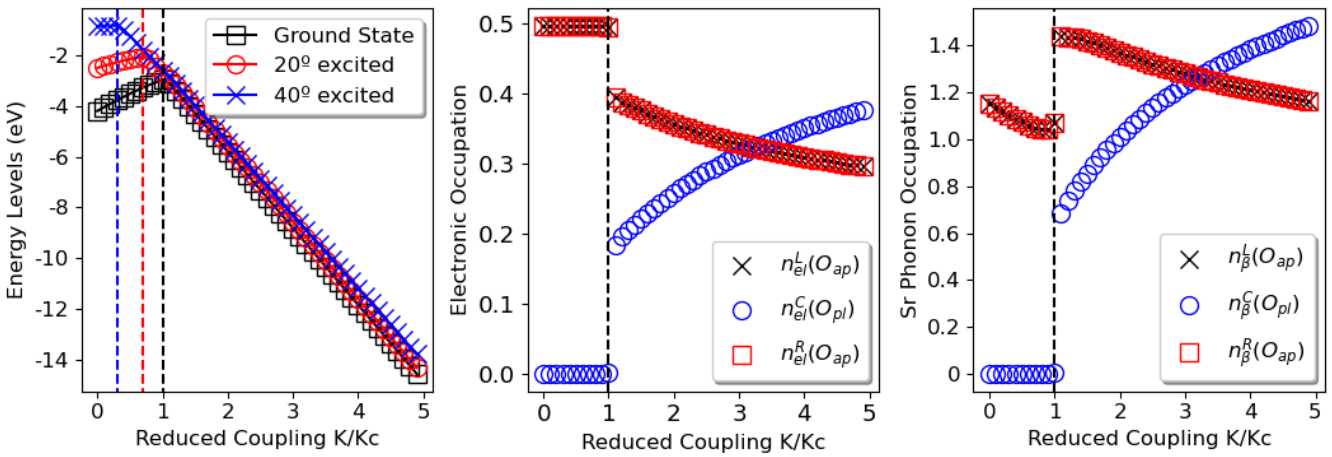

Figure 3. *Left*: The ground state energy of the 6-atom cluster Hamiltonian as a function of reduced anharmonicity, K/K_c, for the non-adiabatic, intermediate λ coupling regime where lateral polarons are already formed – black (squares) ground state, red (circles) 20th excited state, blue (crosses) 40th excited state. The critical coupling, K_c, becomes smaller for higher excited states indicating that these synchronize more easily than the ground state. *Center*: The electronic occupations for left/right O_{ap} (black/red squares/crosses) as well as for the central O_{pl} (blue circles), as a function of reduced anharmonicity, K/K_c of the ground state. As anharmonicity crosses the critical value, charge begins to be pumped from the apical oxygens reservoirs into the planes. *Right* The phonon occupations for left/right sites (overlapping black/red square/cross) as well as for the central oxygen site (blue circles), as a function of reduced K/K_c anharmonicity, of the ground state. A new planar deformation (blue circles) becomes active at the critical anharmonicity, together with the pumping of charge – a novel (planar) IQTP is formed.

we proceed by applying three different techniques.

A. The first order synchronization phase transition

As demonstrated in appendix A, the set of coupled equations of motion for the vibrational degrees of freedom obtained from the Hamiltonian (1)-(4) can be conveniently rewritten, within a mean field approximation [45–47], as a single, first–order differential equation for the phases of the oscillators, θ_i, in which temperature effects can be added by introducing a white thermal noise, $\zeta_i(t)$, thus providing, in terms of the Kuramoto's complex order parameter $re^{i\Psi}$

$$\dot{\theta} = \omega_i + Kr^2 \sin\left[\theta_i(t) + \psi\right] + \xi_i(t) \tag{6}$$

such that $\langle \zeta_i(t) \rangle = 0$ and $\langle \zeta_i(t)\zeta_i(t') \rangle = 2\gamma k_B T \delta_{ij} \delta(t - t')$, where γ is a damping constant. The solution to such first order equations yields

$$r = \sqrt{1 - \frac{K_c(\delta, T)}{rK}} \tag{7}$$

unveiling the first order nature of the synchronization transition that occurs at $K_c(\delta, T)$, a critical coupling that is determined both by the temperature T as well as a quenched spread δ that relates to disorder.

B. The formation of a planar IQTP

The exact diagonalization results also show that not only the total Sr-phonon occupation jumps at K_c but also, most interestingly, an unexpected Sr-phonon central occupation, $n_\beta(C)$, appears above the first order anti-phase synchronization transition. This observation motivated us to redefine the $O_{ap}-Sr-O_{ap}$ triatomic molecule term of the original Hamiltonian (4) as:

$$H_{Sr} = \sum_r \hbar\Omega_{Sr}\beta_r^\dagger\beta_r + K\left(\beta_C^\dagger b_L b_R + \beta_C b_L^\dagger b_R^\dagger\right), \tag{8}$$

where $\beta_r, \beta_r^\dagger$ are now to be understood as the projection of the triatomic molecular vibration at the relevant sites of the cluster, namely $r = L, C, R$, Lin's states $|11010\rangle, |01110\rangle$ and $|01011\rangle$, respectively. When compared to the initial Hamiltonian, this description of the molecule shows that the only source of anharmonicity comes from the projection of molecular phonons in the central, planar site of the cluster, Opl, represented by $\beta_C(\beta_C^\dagger)$, which is motivated by the numerical results.

After a multimodal, nonlinear Bogoliubov transformation discussed in Appendix B, the total diagonal phonon Hamiltonian in terms of new Bogoliubov phonons can be written as

$$H'_d = \sum_r \hbar F(K) B^\dagger_{r+C} B_{r+C} \tag{9}$$

and anharmonicity-dependent, novel, central phonon

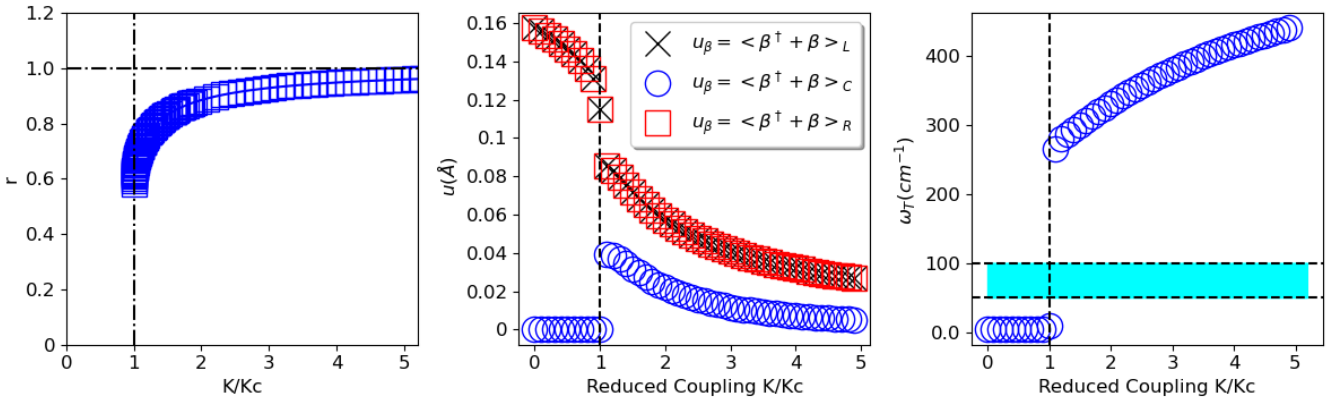

Figure 4. *Left*: The solution to Kuramoto's order parameter equation (7) as a function of the reduced coupling in the ground state, showing that indeed a first order synchronization phase transition takes place. *Center*: The expectation values of the $\mathrm{Cu}(2) - \mathrm{O_{ap}}$ displacement from the average position, where the contributions for u_L comes from the left (black crosses) Lin states $|11010\rangle$ and for u_R from the right (red squares) Lin states $|01011\rangle$. For u_C, the expectation values receive contribution from the central (blue circles) Lin states $|01110\rangle$, showing the Sr-related phonons projection in the $\mathrm{CuO_2}$ plane. *Right*: The polaron tunneling frequency (blue circles), defined as the difference in energy between the first excited and the ground states, $\hbar\omega_T = E_1 - E_0$, is shown as a function of the reduced coupling at the ground state. It shows a jump at the critical coupling, indicating the value of the anharmonicity beyond which the initially frozen polarons become an IQTP, allowed to quantum tunnel internally between the two lateral positions in the cluster. Notice that the tunneling frequency keeps increasing for larger anharmonicity, which is a signature of nonlinear dynamics. The shaded area represents the expected range of experimental values for the ITQP tunneling frequency

modes are present, whose natural frequencies $\hbar F(K)$ are given by the expression

$$\hbar F(K) = \frac{\hbar\omega}{A}\left[\frac{\omega}{\Omega}n_\beta(C) + \frac{\hbar\omega - \hbar\Omega}{2\hbar\Omega}\right] + \frac{K\sqrt{n_\beta(C)}}{A}\frac{\left[(\hbar\omega)^2 - (\hbar\Omega)^2\right]^{1/2}}{2\hbar\Omega}\left(1 + 2n_\beta(C)\right) \tag{10}$$

We have found that, before synchronization, $K < K_c$, $\hbar F(K) = 0$ because $n_\beta(C) = 0$, so this term vanishes and is actually valid solely for $K \gg K_c$. The multimodal, nonlinear Bogoliubov transformation needs also to be applied to the original electron-phonon coupling and, in the limit of strong anharmonicity, together with equation (9), can be written as

$$H'_{Sr} = \sum_r hF B^\dagger_{r+C} B_{r+C} - \sum_r \lambda' n_r \left(B_{r+C} + B^\dagger_{r+C}\right) \tag{11}$$

and the new excess-hole-central-phonon coupling is given by

$$\lambda' = \lambda\sqrt{\frac{n_\beta(C)}{A}}\left(\sqrt{\frac{\omega+\Omega}{2\Omega}} + \sqrt{\frac{\omega-\Omega}{2\Omega}}\right) \tag{12}$$

Thus, we can conclude that after the synchronization of the left and right O_{ap} vibrations, the transition to a synchronized IQTP's phase, the pumping of charge and phonon projection to the $\mathrm{CuO_2}$ plane promotes the formation of an IQTP in the central, planar site. This is corroborated by the finite displacement calculated from the projection of the triatomic molecular phonons, controlled by $\beta(\beta^\dagger)$, in the planar site, associated to the planar oxygen Opl (Fig. 4b). Before the synchronization transition, the left/right phonons causes independent oscillations of the apical oxygens, controlled by $b_L(b_L^\dagger)$,$b_R(b_R^\dagger)$, but with a non-zero contribution coming also from the projection of the molecular phonons into the left/right sites (Fig. 4b, overlapping square/cross symbols). This is evident when we look to the anharmonic term in the original Hamiltonian Eq. (4), where any finite value of K will contribute to the exchange of molecular vibrations and independent left/right oscillations. When $K > K_c$, on the other hand, a finite projection of the triatomic molecular vibration appears in the central site (Fig. 4b), blue circles), and the otherwise independent oscillations associated to the left/right apical oxygens will now be controlled solely by the triatomic molecular vibration, since its phases are locked, as shown by the Kuramoto analysis above. Therefore, a planar IQTP arises from the synchronization transition.

C. The triple-well

The triple-well structure can now be elucidated. Before synchronization, $K < K_c$, we have $\sqrt{n_\beta(C)} = 0$ and the harmonic part, H'_d, of the total transformed Hamiltonian contains simply two decoupled harmonic vibrations, one for each of the possible $\pm r + r'' = L, R$ combinations, respectively, thus composing a double-well structure, see Fig. 5a). In this case the single excess hole in the cluster is found either at the

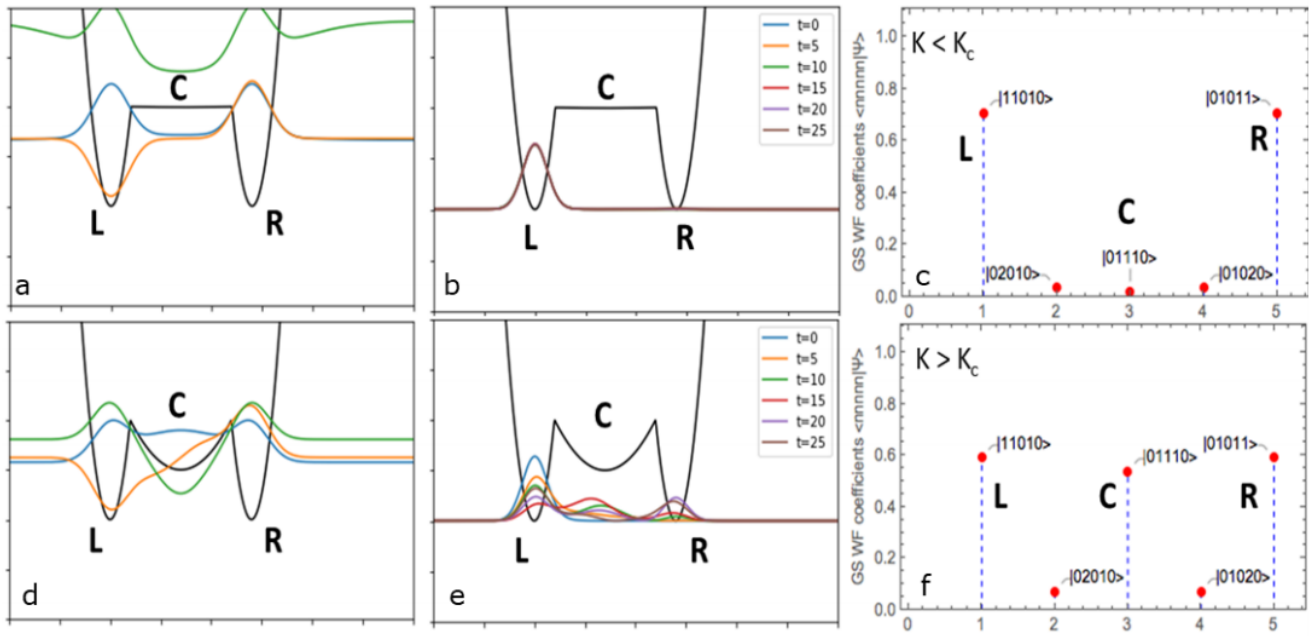

Figure 5. a) For $K < K_c$, the potential (black) depth and width are large and the symmetric (blue) and anti-symmetric (orange) components of the lateral ground state wave function are degenerate, while a central excited state (green) is too energetic to support tunneling. b) The absence of tunneling of the polarons in this scenario is demonstrated by its fixed position over time. c) The IQTP localization is also observed in the ground state wavefunction coefficients that are nonzero at its fixed location on either the left or right sides and vanish at the central position. d) for $K > K_c$ the symmetric (blue) and anti-symmetric (orange) solutions of the wave function become non-degenerate and the central well on the planar oxygen site in the synchronized phase substantially lowers the energy of the excited state (green), forming an anharmonic structural adiabatic passage (ASAP) that promotes tunneling between left and right IQTPs. This results in the nonzero tunneling frequency of the synchronized phase. The colors are identical with (a). e) Due to the ASAP the IQTP is now observed to tunnel from left to right through the center as time evolves. f) The electronic occupation at the central, planar atom becomes nonzero upon synchronization. Small but finite occupation of the excess hole also occurs on the two Cu sites, demonstrating delocalization throughout the cluster.

(L) or (R) apical oxygen atoms. Once the system is prepared, say, at the (L) position it remains at that position even after time evolves, as shown explicitly in Fig. 5b). This results from the absence of a tunneling frequency for $K < K_c$ as obtained from our exact diagonalization studies and as shown in Fig. 4c). The ground state wave function coefficients given in Fig. 5c) shows finite occupation at the lateral positions, Lin's states $|11010\rangle$ and $|01011\rangle$, and zero electronic occupation at the central position, $|01110\rangle$, for $K < K_c$. After synchronization, $K > K_c$, however, we have $\sqrt{n_\beta(C)} \neq 0$ and the harmonic part of the transformed Hamiltonian contains three coupled harmonic parts, one for each of the possible $\pm r + r'' = L, C, R$ combinations, respectively, thus composing a three-well structure, see Fig. 5d). In this case the single excess hole in the cluster can be found at all (L), (R) and (C) oxygen atoms. If the system is prepared, say, at the (L) position the existence of a finite tunneling frequency shows that the wave function evolves with time and the excess hole becomes delocalized. This is depicted in Fig. 5e). This results from the sudden emergence of a nonzero tunneling frequency for $K > K_c$ as shown in Fig. 4c). The ground state wave function coefficients given in Fig. 5f) shows finite but decreasing occupations at the lateral positions, Lin's states $|11010\rangle$ and $|01011\rangle$, and nonzero, increasing electronic occupation at the central position, $|01110\rangle$, for $K > K_c$.

The electron-phonon part, H'_{el-ph} of the total Hamiltonian also contains three distinct couplings, two for the lateral apical oxygen atoms at L and R, and one at the central oxygen atom through the coupling

$$\lambda\,(n_C - 1)\,\sqrt{n_\beta(C)} \tag{13}$$

We now see how both the central electronic occupation, n_C, and the central Sr-phonon occupation, $n_\beta(C)$, evolve simultaneously after the synchronization transition for $K > K_c$. As the coupling increases and we reach the first order phase transition, the electronic occupation of the central site, together with the presence of a novel central phonon, give rise to a planar IQTP, related to the coupling of these two entities. Fig. 5d) shows the effect of electronic occupation in the central site: a middle well is now present and promotes the splitting between the symmetric and anti-symmetric solution. Acting like an anharmonic structural adiabatic passage (ASAP), Fig. 5e) shows the middle well developing tunneling for the IQTP's from the left to the right, passing through the central position as a function of time. Finally, Fig. 5f) shows the coefficient weights of electronic wave function for the ground state after the synchronization transition, where is clear that the extra charge of

the cluster is now delocalized, since the central position has a non-zero contribution.

IV. CONCLUSION

An essential aspect of this application of the Kuramoto model is that the IQTPs are not a construct of virtual or model oscillators [46] but reside, upon doping, in a specific crystal environment. Our calculations were performed on physical quantum objects, namely atoms strongly coupled by bonds specific to each pair where the interaction is nonlinear and asymmetric and the oscillations are quantized, constituting a complex three-dimensional network. Since these initial calculations are limited to a minimal set of atoms they do not take into consideration the addition within the square geometry motif of more atoms to enlarge the synchronized domain. Such an extended array could accommodate ratios of holes, $\mathrm{O_{ap}}$ both larger and smaller than $1/2$, posing the question of the limits of, and effects on, the synchronization in the extended systems. A second simplification of our model is its neglect of the complications of additional degrees of freedom in real materials, e.g., charge, spin, etc. [48], including their contributions to the dissipation of the synchronization that determines its phase diagram. In this first set of calculations we have used a simple generic form for dissipation. An important difference in the treatment of IQTP synchronization in crystals versus other oscillator systems is that their constituent atoms possess a high degree of symmetry. The transition from the unsynchronized to the synchronized phase increases this symmetry. In condensed phases, however, it is determined by the locations of the atoms in the static structures. Here the formation and breaking of the symmetry is an attribute of the dynamics.

These open questions demonstrate the potential value of the approach presented in this work, in addition to its utility in capturing some of the consequences of IQTPs. If IQTPs have an important function in the HTSC mechanism [28], the question is what that would be? One possibility is that the IQTP provides a strong, highly polarizable, local mode, driven to a nonlinear, non-thermal regime by the coupling to quantum tunneling, which enhances SC pairing [49]. Although we do not necessarily imply that the synchronization transition drives a simultaneous SC one, an intriguing possibility, we note that since T_c is closely correlated with the hole density on the O atoms of the $\mathrm{CuO_2}$ planes [50, 51], the delocalization of the hole from $\mathrm{O_{ap}}$ (and by extension from the charge reservoir) into $\mathrm{O_{pl}}$ in the synchronized state substantially influences this parameter. This involves another outstanding problem, namely connecting the charge and dynamics of the $\mathrm{Cu-O_{ap}}$ IQTP to the entire copper oxide plane and its complexity [52]. We can also now understand the shifts of the tunneling frequency with temperature as an effect of feedback from the hole density on $\mathrm{O_{pl}}$ to the IQTP after its incorporation into the triple-well state. Although the microscopic nature of the pairing interaction in superconducting cuprates remains unresolved, the experimental evidence for at least coupling to the lattice is incontrovertible [37, 53]. This introduces the possibility that a more generic, low temperature SC mechanism is enhanced by phonons via, e.g., coupling to specific displacement modes [48] including ones on the c axis [31, 54], or exchange with a second, shallow, electronic band [55–57] that generates screening of otherwise detrimental superconducting fluctuations allowing higher temperature superconductivity [58, 59]. Recent experiments indicate that dynamic effects are key. One that emphasizes the often noted c-oriented character of such enhancements is the induction of transient superconducting behavior by coherent IR excitation along the c axis [60–62]. Momentum-resolved electron energy-loss spectroscopy (MEELS) measurements of the dynamic charge response [63, 64] show that the temperature dependence of the spectral weight at $0.1-0.5\ eV$, that in underdoped $\mathrm{Bi_2Sr_2CaCu_2O_{8+\delta}}$ is large and increases with decreasing temperature, favoring CDW formation, is reduced and decreases at lower temperatures in an overdoped sample. The so-called strange metal region thus occurs in optimally doped samples and its relatively low spectral weight in that region is constant from $23-300\ K$ [65]. It is intriguing to compare this with ARPES experiments on the same compound whose analogous increase of the superconducting gap-to-T_c ratio from over- to optimally doped regimes was interpreted as a synergy between the electron-phonon coupling and electronic interaction in the strange metal [36]. The broad momentum distribution observed with MEELS is consistent with a local mode such as an IQTP.

Whatever mechanism(s) proves correct, there is agreement that new physics of complex quantum systems is called for [65, 66]. IQTP synchronization meets that requirement. The basis for the charge-ordered states is the localized charge inhomogeneities that interact within and with the scaffolding of their host lattice, posing the question of the origin of the great variety of behaviors. Static disorder from lattice defects and the consequent division of the crystal into domains on the scale of the defect separation could accomplish this. However, although such disorder is known to boost the superconductivity [67], the implication that disorder is a principal factor rather than one of many is inconsistent with the absence of a quantitative correlation. A notable characteristic of the $\mathrm{Cu-O_{ap}}$ IQTPs observed in EXAFS and their coupling to the superconductivity is that all of the pairs are at one of the two distances. Since the simple presence of the IQTPs is therefore insufficient, the determining factor would be the organization of their collective dynamics by Kuramoto-like synchronization mechanisms. Our six-atom model demonstrated that even two coupled IQTPs control the charge distribution between the planes and reservoir. In addition to this key step occurring in the so-called dielectric layer [54] is the local, quantum entanglement of the charges. The subsequent combination of domain sizes and shapes that would be consistent with the same arrangement of defects, the density of holes within the domains, and temperature that determines the order parameter and lifetimes of the synchronized phases would clearly produce a wide range of behaviors.

ACKNOWLEDGEMENTS

The authors acknowledge the financial support from the Slovenian Research Agency (core funding No. P1-0040). Work at Washington State University is partially supported by the US National Science Foundation Division of Materials Research Early Concept Grants for Exploratory Research Grant 1928874. Use of the Stanford Synchrotron Radiation Lightsource, SLAC National Accelerator Laboratory, is supported by the US Department of Energy, Office of Science, Office of Basic Energy Sciences Contract DE-AC02-76SF00515. VV and MBSN acknowledge the financial support of CAPES and FAPERJ.

Appendix A: Kuramoto's synchronization transition

We start by providing meaning to the first order transition. To this end, we shall make use of a mean field approximation to treat the anharmonic three-phonon term in Eq. (4). For convenience, first we rescale the anharmonic coupling $K \to K/N$, where N represents the number of different oscillators (phonons) at each of the two kinds of oscillator communities: left (L) and right (R) oscillators. Second, since all oscillators are bosons we introduce a mean field approximation in terms of which the triatomic molecular phonon population can be written as $\langle \beta^\dagger \beta \rangle = |R|^2 = \langle \beta^\dagger \rangle \langle \beta \rangle = R^* R \neq 0$, where R plays the role of a complex order parameter. Now, the Heisenberg's equations of motion derived from Hamiltonian (1)-(4) for $i = L, R$ phonons read

$$\begin{aligned} i\frac{db_i}{dt} &= \omega_i \left(b_i - \frac{\lambda n_i}{\hbar\omega} \right) + \frac{KR}{N\hbar} b_j^\dagger \\ -i\frac{db_i^\dagger}{dt} &= \omega_i \left(b_i^\dagger - \frac{\lambda n_i}{\hbar\omega} \right) + \frac{KR^*}{N\hbar} b_j \end{aligned} \tag{A1}$$

So far, this is a set of coupled operatorial differential equations. Let us take the quantum mechanical expectation value at both sides of the above equations, and recall that phonon coherent states are eigenstates of the anihilation operator $b_{i,j}|z_{i,j}\rangle = z_{i,j}|z_{i,j}\rangle$. We then drop all constant terms that simply provide an overall shift of the equilibrium position and write the complex numbers $z_{i,j} = z_0 e^{-i\theta_{i,j}(t)}$, where we have made the assumption that the amplitudes of the phonons L and R are equal, z_0, and only their phases change. Finally we introduce Kuramoto's complex order parameter, $R = re^{i\psi}$, where r is the real part of R and ψ it's an arbitrary phase. Furthermore, we choose $R = -ir$, as purely imaginary, so that after combining the two equations in (A1) we arrive at

$$\frac{d\theta_i(t)}{dt} = \omega_i + \sum_{j=L,R} \frac{Kr}{N\hbar} \sin\left[\theta_i(t) + \theta_j(t)\right]. \tag{A2}$$

We recognize the dynamical problem in (A2) as a Kuramoto's differential equation for anti-phase synchronization $\theta_i \to -\theta_j$. The mean field version of the above equation is obtained as usual, by introducing the order parameter [45] $re^{i\psi} = 1/N \sum_{j=1}^{N} e^{i\theta_j}$. Here the real part r plays the role of the coherence amplitude for a population of N phase oscillators and ψ indicates the coherence phase. Kuramoto's mean field equation can then finally be written as

$$\theta_i(t) = \omega_i + Kr^2 \sin\left[\theta_i(t) + \psi\right], \tag{A3}$$

where from now on we set $\hbar = 1$. According to equation (A3), phase locking occurs for $\theta_i \to -\psi$, and as such the anti-phase synchronization favoured by equation (A2) implies $\theta_j \to \psi$. Now, since we have chosen before $\psi = -\pi/2$ (such that $R = re^{i\psi} = -ir$) we end up with $\theta_i + \theta_j = 0$ and $\theta_i - \theta_j = -\pi$, which reflects the anti-phase synchronization transition.

Once we established the anti-phase character of the synchronization transition, we now show its first order nature. For that, the mean field analysis initiated above for the Kuramoto model needs to be supplemented by a self consistency equation [45] such as

$$1 = Kr \int_{-\frac{\pi}{2}}^{\frac{\pi}{2}} \cos^2\theta g\left(Kr^2 \sin\theta\right) d\theta, \tag{A4}$$

where $g(\omega)$ is a symmetric Lorentzian distribution of frequencies with quenched spread δ given by

$$g(\omega) = \frac{1}{\pi} \frac{\delta}{\omega^2 + \delta^2}. \tag{A5}$$

Solving the self consistent equation, one finds for the order parameter

$$r = \sqrt{1 - \frac{K_c(\delta)}{Kr}}, \tag{A6}$$

where $K_c(\delta) = 2\delta$ is the critical coupling in terms of a quenched spread δ.

Finally, since we would like also to incorporate thermal effects to the synchronization transition, we recall that temperature effects can be added to the problem by introducing a thermal noise

$$\theta = \omega_i + Kr^2 \sin\left[\theta_i(t) + \psi\right] + \xi_i(t), \tag{A7}$$

such that $\langle \xi_i(t) \rangle = 0$ and $\langle \xi_i(t)\xi_j(t') \rangle = 2\gamma k_B T \delta_{ij} \delta(t - t')$, where γ is a damping constant. In this case, the oscillator probability density ρ must satisfy the nonlinear Fokker-Planck equation [45]

$$\begin{aligned} \frac{\partial \rho}{\partial t} &= D\frac{\partial^2 \rho}{\partial \theta^2} - \frac{\partial (v\rho)}{\partial \theta} \\ v &= \omega + Kr^2 \sin\left[\theta_i(t) + \psi\right] \end{aligned} \tag{A8}$$

where v is the drift velocity and with $D(\Omega) = \gamma k_B T \Omega$ is a diffusion coefficient. The solution to these coupled equations yields

$$r = \sqrt{1 - \frac{K_c(\delta, T)}{Kr}}, \tag{A9}$$

and we see that the only difference to equation (A6) is in the critical coupling, which now reads

$$\frac{2}{K_c(\delta, T)} = \int_{-\infty}^{+\infty} d\Omega \frac{g(D(\Omega) + \omega)}{\Omega^2 + 1}. \tag{A10}$$

The important conclusion here is that the overall effect of temperature (dissipation through thermal noise) is to increase the critical coupling K_c making it harder for the oscillators to synchronize. From the mathematical point of view the situation is clear: temperature increases the spread in the Lorenztian probability distribution for the oscillators and this leads to an increase of the critical anharmonicity for synchronization. From the physical point of view the situation is also clear: temperature, introduced in connection to dissipation enhances decoherence, which also leads to an increase of the critical coupling for synchronization. Elevating the temperature does not alter the character of the synchronization transition, it remains first order.

Appendix B: The nonlinear multimodal Bogoliubov transformation

The correlated, anharmonic phonon Hamiltonian (1)-(4) of the main text can be diagonalized by means of a multi-modal, nonlinear Bogoliubov transformation. To this end we introduce new phonons B_r,$B_r^\dagger$ that connect to the original ones through

$$\begin{aligned} b_r &= \sum_{r''} \left(u^*_{r,r''} \beta_{r''} B_{r+r''} + v_{r,r''} \beta^\dagger_{r''} B^\dagger_{-r+r''} \right) \\ b^\dagger_r &= \sum_{r''} \left(u_{r,r''} \beta^\dagger_{r''} B^\dagger_{r+r''} + v^*_{r,r''} \beta_{r''} B_{-r+r''} \right) \end{aligned} \tag{B1}$$

It is important to emphasize that, while r, labelling the original b_L,b_R phonons runs over L,R only, here r'' is allowed to run over all three oxygen positions: L, R, and C. This is what provides the transformation with a multimodal character. The nonlinear aspect results from the presence of quadratic terms such as $\beta_{r''} B_{r+r''}$.

Unitarity of the Bogoliubov transformation guarantees that the original commutation relations are preserved. We started with L and R phonons only, satisfying the commutation relations

$$\left[b_r, b^\dagger_{r'} \right] = \delta_{r,r'}, \quad r, r' = L, R \tag{B2}$$

For the sake of clarity let us consider the case where $r = r'$, in which case $[b_r, b_r^\dagger] = 1$, and let us impose the bosonic comutation relations

$$\begin{aligned} \left[B_{\pm r+r''}, B^\dagger_{\pm r+r'''} \right] &= \delta_{r'',r'''} \\ \left[\beta_{r''}, \beta^\dagger_{r'''} \right] &= \delta_{r'',r'''} \end{aligned} \tag{B3}$$

and expectation values of all phonon operators

$$\begin{aligned} n_\beta (r'') &= \left\langle \beta^\dagger_{r''} \beta_{r''} \right\rangle, \\ n_B (\pm r + r'') &= \left\langle B^\dagger_{\pm r+r''} B_{\pm r+r''} \right\rangle, \end{aligned} \tag{B4}$$

the unitarity of the transformation reduces to a sum rule

$$\begin{aligned} \left[b_r, b^\dagger_r \right] &= \sum_{r''} |u_{r,r''}|^2 \left[1 + n_\beta (r'') + n_B (r + r'') \right] \\ &- \sum_{r''} |v_{r,r''}|^2 \left[1 + n_\beta (r'') + n_B (-r + r'') \right] = 1. \end{aligned} \tag{B5}$$

After performing the Bogoliubov transformation one must as usual eliminate the nonlinear, anharmonic interaction by setting to zero the equation for the off-diagonal Bogoliubov coefficients, which in our case takes the form

$$\begin{aligned} &\sum_{r,r'',r'''} \left[\left\langle \beta^\dagger_{r''} \beta_{r'''} \right\rangle \Big(\hbar\omega u_{r,r''} v_{r,r''} \right. \\ &\left. + K \sqrt{n_\beta(C)} \left(v_{r,r''} v_{-r,r''} + u_{r,r''} u_{-r,r'''} \right) \Big) \right] = 0 \end{aligned} \tag{B6}$$

At this point some approximations are in order. First, we use that $v_{-r,r'} = v^*_{r,r'}$ and the same for the other Bogoliubov coefficients. From the numerical results of the exact diagonalization, we know that the Sr-phonon occupation in the central position increases, while the left and right contributions decrease after the critical coupling. Thus, we shall restrict our subsequent analysis to the strong anharmonicity case, $K \gg K_c$, and approximate

$$\left\langle \beta^\dagger_{r''} \beta^\dagger_{r''} \right\rangle \approx \left\langle \beta^\dagger_{r'} \right\rangle \left\langle \beta^\dagger_{r''} \right\rangle = \sqrt{n_\beta(C)} \sqrt{n_\beta(C)} \delta_{r'',C} \delta_{r''',C}$$

which is basically the same approximation we have already used when discussing Kuramoto's mean field equation. Using these approximations, and after eliminating the coefficients associated with the off-diagonal part of the transformed Hamiltonian, we are left with

$$\sum_r n_\beta(C) \left[\hbar\omega u_{r,C} v_{r,C} + K \sqrt{n_\beta(C)} \left(|v_{r,C}|^2 + |u_{r,C}|^2 \right) \right] = 0$$

Solving for the expression inside square brackets we obtain the Bogoliubov coefficients

$$u_{r,C} = \frac{1}{\sqrt{A}}\left(\frac{\omega+\Omega}{2\Omega}\right)^{\frac{1}{2}}$$
$$v_{r,C} = \frac{1}{\sqrt{A}}\left(\frac{\omega-\Omega}{2\Omega}\right)^{\frac{1}{2}} \tag{B7}$$

where $\hbar\Omega = \sqrt{((\hbar\omega)^2 - 4K^2 n_\beta(C))}$ and $A = 1 + n_\beta(r+C) + n_\beta(C)$. Now we are ready to write down the total diagonal phonon Hamiltonian in terms of the new Bogoliubov phonons as

$$H'_d = \sum_r \hbar F(K) B^\dagger_{r+C} B_{r+C} \tag{B8}$$

where the natural frequencies $\hbar F$ are given by the expression

$$\hbar F(K) = \frac{\hbar\omega}{A}\left[\frac{\omega}{\Omega} n_\beta(C) + \frac{\hbar\omega - \hbar\Omega}{2\hbar\Omega}\right] + \frac{\kappa\sqrt{n_\beta(C)}}{A}\frac{\left[(\hbar\omega)^2 - (\hbar\Omega)^2\right]^{\frac{1}{2}}}{2\hbar} \tag{B9}$$

We can see that, before synchronization, $K < K_c$, $\hbar F = 0$, because $n_\beta(C) = 0$, and is actually valid only for $K \gg K_c$. We must also consider the effect of the Bogoliubov transformation in the original electron-phonon coupling of the Hamiltonian. In terms of the new phonon operators we have

$$b_r + b^\dagger_r = \sum_{r''} \sqrt{n_\beta(C)}\Big[\left(u^*_{r,r''} B_{r+r''} + u_{r,r''} B^\dagger_{r+r''}\right) + \left(v^*_{r,r''} B_{-r+r''} + v_{r,r''} B^\dagger_{-r+r''}\right)\Big] \tag{B10}$$

And we have used the same approximation for the occupation of β phonons. Splitting the sum in $r'' = L, R, C$ into a lateral (L and R) and central (C) contributions, in other words, writing the transformed electron-phonon Hamiltonian as $H'_{el-ph} = H^{lateral}_{el-ph} + H^{central}_{el-ph}$, in the limit of strong coupling $K >> K_c$, where we can look only at the central contributions, we write

$$H^{central}_{el-ph} = \sum_r \lambda n_r \sqrt{n_\beta(C)}\,(u_{r,c} + v_{r,c})\left(B_{r+C} + B^\dagger_{r+C}\right)$$

Where we used the inversion symmetry around the central position to simplify the coefficients. Finally, in terms of the Bogoliubov coefficients and together with diagonal part (B8), the newly transformed Hamiltonian with a novel central electron-phonon coupling is written as $H' = H'_d + H^{central}_{el-ph}$

$$H' = \sum_r \hbar F(K) B^\dagger_{r+c} B_{r+c} - \sum_r \lambda' n_r \left(B_{r+c} + B^\dagger_{r+C}\right)$$

Where the new coupling depends on the central Sr-phonon related occupation $n_\beta(C)$ as

$$\lambda' = \lambda\sqrt{\frac{n_\beta(C)}{A}}\left(\sqrt{\frac{\omega+\Omega}{2\Omega}} + \sqrt{\frac{\omega-\Omega}{2\Omega}}\right) \tag{B11}$$

To summarize, by separating the Sr triatomic molecule and using a nonlinear, multi-modal Bogoliubov transformation, we started with two oscillator communities but we ended up with three transformed oscillator communities, associated to the operators $B, B^\dagger$, which mix the original left and right oscillations of the apical oxygens to a novel central phonon, located in the plane, and related to the planar oxygen oscillations. Furthermore, those novel planar vibrational modes couple to the electronic degrees of freedom with a renormalized electron-phonon coupling given by equation (B11), which gives rise to a new IQTP mode, now located in the cooper oxide plane. To see how exactly the new phonon, B_C, couples to the central oxygen atom, Opl, let us recall that within our 6-atom cluster one has a single excess hole for all oxygen atoms

$$n_L + n_R + n_C = 1 \tag{B12}$$

where n_C is the electronic occupation of the planar Opl at the center of the cluster. By symmetry, we expect the Bogoliubov coefficients to satisfy

$$u_{L,C} = u_{R,C} = u_C$$
$$v_{L,C} = v_{R,C} = v_C \tag{B13}$$

so that, after applying the non-linear Bogoliubov transformation we rewrite the central contribution of the electron-phonon transformed Hamiltonian $H^{central}_{el-ph}$ as

$$H^{\text{central}}_{el-ph} = \lambda\,(1 - n_C) \times\sqrt{n_\beta(C)}\left[\left(\left(u_C + v_C\right)^* B_C + \left(u_C + v_C\right) B^\dagger_C\right)\right] \tag{B14}$$

Where the new phonon B_C couples to the central oxygen atom, via its occupation, after the synchronization transition, when $n_\beta(C) > 0$. Therefore, after a multimodal, non-linear Bogoliubov transformation, not only a newly phonon mode, associated to the planar oxygen displacements, appears, but it also couples to the excess charge pumped to the central site, giving rise to an extension of the IQTP's to the plane and allowing the description of the problem to be elegantly summarized in the triple-well interpretation.

[1] W. M. Li *et al*, Superconductivity in a unique type of copper oxide. *Proc. Natl. Acad. Sci. U.S.A.* **116**, 12156-12160 (2019).

[2] S. D. Conradson *et al*, Local lattice distortions and dynamics in extremely overdoped superconducting $YSr_2Cu_{2.75}Mo_{0.25}O_{7.54}$. *Proc. Natl. Acad. Sci. U.S.A.* **117**, 4559-4564 (2020).

[3] S. D. Conradson, Theodore H. Geballe, Changqing Jin, Lipeng Cao, Gianguido Baldinozzi, Jack M. Jiang, Matthew J. Latimer, and Oliver Mueller, Local structure of $Sr_2CuO_{3.3}$, a 95 K cuprate superconductor without CuO2 planes. *Proc. Natl. Acad. Sci. U.S.A.* **117**, 4565-4570 (2020).

[4] S. D. Conradson *et al*, Nonadiabatic coupling of the dynamical structure to the superconductivity in $YSr_2Cu_{2.75}Mo_{0.25}O_{7.54}$ and $Sr_2CuO_{3.3}$. *Proc. Natl. Acad. Sci. U.S.A.* **117**, 33099-33106 (2020).

[5] T. Egami, Real-Space Description of Dynamics of Liquids. *Quantum Beam Sci.* **2**, 22. (2018)

[6] M. I. Salkola, A. R. Bishop, S. A. Trugman, and J. M. Deleon, Correlation-function analysis of nonlinear and nonadiabatic systems - polaron tunneling. *Phys. Rev. B* **51**, 8878-8891 (1995).

[7] J. M. DeLeon, S. D. Conradson, T. Tyson, A. R. Bishop, M. Salkola, F.J. Espinosa and J.L. Pena, .X-ray absorption fine structure applied to the study of systems with lattice instabilities. 189-199. Paper presented at Proceedings of the 1996 MRS Spring Meeting, Boston, MA, USA.

[8] S. D. Conradson, I. D. Raistrick, and A. R. Bishop, Axial oxygen centered lattice instabilities and high-temperature superconductivity. *Science* **248**, 1394-1398 (1990).

[9] J. M. de Leon, S. D. Conradson, I. Batistić, and A. R. Bishop, Evidence for an axial oxygen-centered lattice fluctuation associated with the superconducting transition in $YBa_2Cu_3O_7$. *Phys. Rev. Lett.* **65**, 1675-1678 (1990).

[10] P. G. Allen, J. M. de Leon, S. D. Conradson, and A. R. Bishop, Characterization of a split axial-oxygen site in $TlBa_2Ca_3Cu_4O_{11}$ by extended x-ray-absorption fine-structure spectroscopy. *Phys. Rev. B* **44**, 9480-9485 (1991).

[11] J. M. de Leon, S. D. Conradson, I. Batistić, and A. R. Bishop, Correlation between axial-oxygen anharmonicity and T_c in $YBa_2Cu_3O_7$ and related-compounds. *Phys. Rev. B* **44**, 2422-2425 (1991).

[12] J. M. de Leon, I. Batistić, A. R. Bishop, S. D. Conradson, and S. A. Trugman, Polaron origin for anharmonicity of the axial oxygen in $YBa_2Cu_3O_7$, *Phys. Rev. Lett.* **68**, 3236-3239 (1992).

[13] J. M. de Leon, S. D. Conradson, I. Batistić, A. R. Bishop, I. D. Raistrick, M. C. Aronson, and F. H. Garzon, Axial oxygen-centered lattice instabilities in $YBa_2Cu_3O_7$ - an application of the analysis of extended x-ray-absorption fine-structure in anharmonic systems. *Phys. Rev. B* **45**, 2447-2457 (1992).

[14] C. H. Booth, F. Bridges, J. B. Boyce, T. Claeson, B. M. Lairson, R. Liang, and D. A. Bonn, Comparison of local structure measurements from c-axis polarized XAFS between a film and a single crystal of $YBa_2Cu_3O_{7-\delta}$ as a function of temperature. *Phys. Rev. B* **54**, 9542-9554 (1996).

[15] J. M. de Leon, G. G. Li, S. Conradson, A. Bishop, M. Subramanian and I. Raistrick, Planar oxygen-centered lattice instabilities in Tl-based high-temperature superconductors. *Physica C* **220**, 377-382 (1994).

[16] A. Bianconi, M. Missori, H. Oyanagi, H. Yamaguchi, D. H. Ha, Y. Nishiara and S. Della Longa. The measurement of the polaron size in the metallic phase of cuprate superconductors. *Europhys. Lett.* **31**, 411-415 (1995).

[17] A. Bianconi, N. L. Saini, A. Lanzara, M. Missori, T. Rossetti, H. Oyanagi, H. Yamaguchi, K. Oka, and T. Ito, Determination of the local lattice distortions in the CuO_2 plane of $La_{1.85}Sr_{0.15}CuO_4$. *Phys. Rev. Lett.* **76**, 3412-3415 (1996).

[18] A. Bianconi et al. Stripe structure in the CuO_2 plane of perovskite superconductors. *Phys. Rev. B* **54**, 12018-12021 (1996).

[19] S. D. Conradson, J. M. De Leon and A. R. Bishop, Local phase separation in Tl-based oxide superconductors. *J. Supercond.* **10**, 329-332 (1997).

[20] M. Acosta-Alejandro, J. M. de Leon, S. D. Conradson and A. R. Bishop, Evidence for a local structural change in $La_2CuO_{4.1}$ across the superconducting transition. *J. Supercond.* **15**, 355-360 (2002).

[21] J. M. de Leon, M.Acosta-Alejandro, S. D. Conradson and A. R. Bishop, Change of the in-plane Cu-O bond distribution in $La_2CuO_{4.1}$ across T_c. *J. Phys. Chem. Solids* **69**, 2288-2291 (2008).

[22] H. Oyanagi, C. Zhang, A. Tsukada and M. Naito, Lattice Instability in High-Temperature Superconducting Cuprates: Polarons Probed by EXAFS, *J. Supercond. Nov. Magn.* **22**, 165-168 (2009).

[23] A. P Menushenkov, K. V Klementev, P. V Konarev, A.A Meshkov, S. Benazeth and J. Purans, The double-well oscillating potential of oxygen atoms in perovskite system $Ba(K)BiO_3$: EXAFS - analysis results. *Nuclear Instruments and Methods in Physics Research Section A - Accelerators Spectrometers Detectors and Associated Equipment* **448**, 340-344 (2000).

[24] A. P. Menushenkov and K. V. Klementev, Extended x-ray absorption fine-structure indication of a double-well potential for oxygen vibration in $Ba_{1-x}K_xBiO_3$. *J. Phys.-Condens. Mat.* **12**, 3767-3786 (2000).

[25] V. G. Ivanov, A. A. Ivanov, A. P. Menushenkov, B. Joseph and A. Bianconi, Fe-As Bond Fluctuations in a Double-Well Potential in LaFeAsO. *J. Supercond. Nov. Magn.* **29**, 3035-3039 (2016).

[26] T. Egami *et al*, Local structural anomaly near T_c observed by pulsed neutron-scattering. *Physica C* **185**, 867-868 (1991).

[27] M. Arai, K. Yamada, S. Hosoya, A. C. Hannon, Y. Hidaka, A. D. Taylor and Y. Endoh, Local structural instability of high-T_c oxide superconductors studied by inelastic neutron-scattering. *J. Supercond.* **7**, 415-418 (1994).

[28] C. J. Zhang and H. Oyanagi, Local lattice instability and superconductivity in $La_{1.85}Sr_{0.15}Cu_{1-x}M_xO_4$ (M=Mn, Ni, and Co). *Phys. Rev. B* **79**, 064521 (2009).

[29] H. S. Obhi and E. K. H. Salje, Effect of the metal-superconductor phase-transition and Co doping on the phonon-spectra of $YBa_2Cu_3O_{7-\delta}$. *Physica C* **171**, 547-553 (1990).

[30] B. K. Guttler, E. K. H. Salje, P. Freeman, J. Blunt, M. Harris, T. Duffield, C. D. Ager and H. P. Hughes, Critical-behavior of bulk phonons in $YBa_2Cu_3O_{7-\delta}$ as observed by infrared-absorption spectroscopy. *J. Phys. Condens. Mat.* **2**, 8977-8983 (1990).

[31] N. N. Kovaleva *et al*. c-axis lattice dynamics in Bi-based cuprate superconductors. *Phys. Rev. B* **69**, 054511 (2004).

[32] S. Sugai, H. Suzuki, Y. Takayanagi, T. Hosokawa, and N. Hayamizu, Carrier-density-dependent momentum shift of the coherent peak and the LO phonon mode in p-type high-T_c superconductors. *Phys. Rev. B* **68**, 184504 (2003).

[33] D. Reznik *et al*, Electron-phonon coupling reflecting dynamic

charge inhomogeneity in copper oxide superconductors. *Nature* **440**, 1170-1173 (2006).

[34] T. Cuk, D. H. Lu, X. J. Zhou, Z.-X. Shen, T. P. Devereaux, N. Nagaosa, A review of electron–phonon coupling seen in the high-T_c superconductors by angle-resolved photoemission studies (ARPES). *Physica Status Solidi (b)* **242**, 11 (2005).

[35] W. Meevasana *et al*, Doping dependence of the coupling of electrons to bosonic modes in the single-layer high-temperature $Bi_2Sr_2CuO_6$ superconductor. *Phys. Rev. Lett.* **96**, 157003 (2006).

[36] Y. He *et al*, Rapid change of superconductivity and electron-phonon coupling through critical doping in Bi-2212. *Science* **362**, 62-65 (2018).

[37] A. Lanzara *et al*, Evidence for ubiquitous strong electron-phonon coupling in high-temperature superconductors. *Nature* **412**, 510-514 (2001).

[38] M. Le Tacon *et al*, Inelastic X-ray scattering in $YBa_2Cu_3O_{6.6}$ reveals giant phonon anomalies and elastic central peak due to charge-density-wave formation. *Nat. Phys.* **10**, 52-58 (2014).

[39] L. Chaix *et al*, Dispersive charge density wave excitations in $Bi_2Sr_2CaCu_2O_{8+\delta}$. *Nat. Phys.* **13**, 952–956 (2017)

[40] Y. He *et al*, Persistent low-energy phonon broadening near the charge-order q vector in the bilayer cuprate $Bi_2Sr_2CaCu_2O_{8+\delta}$, *Phys. Rev. B* **98**, 035102 (2018).

[41] A. R. Bishop, D. Mihailovic and J. M. de Leon. Signatures of mesoscopic Jahn-Teller polaron inhomogeneities in high-temperature superconductors. *J. Phys. Condens. Mat.* **15**, L169-L175 (2003).

[42] E. W. Huang, C. B. Mendl, S. Liu, S. Johnston, Hong-Chen Jiang, B. Moritz and T. P. Devereaux, Numerical evidence of fluctuating stripes in the normal state of high-T_c cuprate superconductors. *Science* **358**, 1161-1164 (2017).

[43] S. Kim, X. Chen, W. Fitzhugh and X. Li, Apical Charge Flux-Modulated In-Plane Transport Properties of Cuprate Superconductors. *Phys. Rev. Lett.* **121**, 157001 (2018).

[44] D. Haskel, E. A. Stern, D. G. Hinks, A. W. Mitchell, and J. D. Jorgensen, Altered Sr environment in $La_{2-x}Sr_xCuO_4$. *Phys. Rev. B* **56**, R521-R524 (1997).

[45] J. A. Acebrón, L. L. Bonilla, C. J. Pérez Vicente, F. Ritort, and R. Spigler, The Kuramoto model: A simple paradigm for synchronization phenomena. *Rev. Mod. Phys.* **77**, 137-185 (2005).

[46] V. Velasco and M. B. Silva Neto, Unconventional superconductivity as a quantum Kuramoto synchronization problem in random elasto-nuclear oscillator networks. *J. of Phys. Comm.* **5**, 015003 (2021).

[47] D. Witthaut, S. Wimberger, R. Burionim and M. Timme, Classical synchronization indicates persistent entanglement in isolated quantum systems. *Nat. Comm.* **8**, 14829 (2017)

[48] S. Johnston, F. Vernay, B. Moritz, Z.-X. Shen, N. Nagaosa, J. Zaanen, and T. P. Devereaux, Systematic study of electron-phonon coupling to oxygen modes across the cuprates. *Phys. Rev. B* **82**, 064513 (2010).

[49] R. C. Dynes, Oxide superconductors - light on a continuing mystery. *Proc. Natl. Acad. Sci. U.S.A.* **118**, e2024422118 (2021).

[50] D. Rybicki, M. Jurkutat, S. Reichardt, C. Kapusta and J. Haase, Perspective on the phase diagram of cuprate high-temperature superconductors. *Nat. Commun.* **7**, 11413 (2016).

[51] M. Jurkutat, A. Erb and J. Haase, T_c and Other Cuprate Properties in Relation to Planar Charges as Measured by NMR. *Condens. Matter* **4**, 67 (2019).

[52] S. Agrestini, N. L. Saini, G. Bianconi and A. Bianconi, The strain Of CuO_2 lattice: the second variable for the phase diagram of cuprate perovskites. *J. Phys. A Math. Gen.* **36**, 9133-9142 (2003).

[53] G.-H. Gweon, T. Sasagawa, S. Y. Zhou, J. Graf, H. Takagi, D.-H. Lee and A. Lanzara, An unusual isotope effect in a high-transition-temperature superconductor. *Nature* **430**, 187-190 (2004).

[54] E. S. Bozin, A. Huq, Bing Shen, H. Claus, W. K. Kwok, and J. M. Tranquada, Charge-screening role of c-axis atomic displacements in $YBa_2Cu_3O_{6+x}$ and related superconductors. *Phys. Rev. B* **93**, 054523 (2016).

[55] A. Bianconi. Multiband superconductivity in high T_c cuprates and diborides. *J. Phys. Chem. Solids* **67**, 567-570 (2006).

[56] H. Keller, A. Bussmann-Holder, and K. A. Muller, Jahn-Teller physics and high-T_c superconductivity. *Mater. Today* **11**, 38-46 (2008).

[57] D. Innocenti, N. Poccia, A. Ricci, A. Valletta, S. Caprara, A. Perali, and A. Bianconi. Resonant and crossover phenomena in a multiband superconductor: Tuning the chemical potential near a band edge. *Phys. Rev. B* **82**, 184528 (2010).

[58] L. Salasnich, A. A. Shanenko, A. Vagov, J. Albino Aguiar, and A. Perali, Screening of pair fluctuations in superconductors with coupled shallow and deep bands: A route to higher-temperature superconductivity. *Phys. Rev. B* **100**, 064510 (2019).

[59] T. T. Saraiva, P. J. F. Cavalcanti, A. Vagov, A. S. Vasenko, A. Perali, L. Dell'Anna, and A. A. Shanenko, Multiband Material with a Quasi-1D Band as a Robust High-Temperature Superconductor. *Phys. Rev. Lett.* **125**, 217003 (2020).

[60] W. Hu *et al*, Optically enhanced coherent transport in $YBa_2Cu_3O_{6.5}$ by ultrafast redistribution of interlayer coupling. *Nat. Mater.* **13**, 705-711 (2014).

[61] R. Mankowsky *et al*, Optically induced lattice deformations, electronic structure changes, and enhanced superconductivity in $YBa_2Cu_3O_{6.48}$. *Structural Dynamics* **4**, 044007 (2017).

[62] A. Cavalleri. Photo-induced superconductivity. *Contemp. Phys.* **59**, 31-46 (2018).

[63] A. Kogar *et al*, Signatures of exciton condensation in a transition metal dichalcogenide. *Science* **358**, 1314-1317 (2017).

[64] S. Vig *et al*, Measurement of the dynamic charge response of materials using low-energy, momentum-resolved electron energy-loss spectroscopy (M-EELS). *SciPost Phys.* **3**, 026 (2017)

[65] M. Mitrano *et al*, Anomalous density fluctuations in a strange metal. *Proc. Natl. Acad. Sci. U.S.A.* **115**, 5392-5396 (2018).

[66] I. Bozovic, X. He, J. Wu and A. T. Bollinger, The Vanishing Superfluid Density in Cuprates-and Why It Matters. *J. Supercond. Nov. Magn.* **31**, 2683-2690 (2018).

[67] D. Pelc, M. Vučković, M. S. Grbić, M. Pozek, G. Yu, T. Sasagawa, M. Greven and N. Barisic, Emergence of superconductivity in the cuprates via a universal percolation process. *Nat Commun.* **9**, 4327 (2018)